Phase Transitions between Different Spin-Glass Phases and between Different Chaoses in Quenched Random Chiral Systems

Tolga Çağlar[1] and A. Nihat Berker[2,3]

[1]*Faculty of Engineering and Natural Sciences, Sabancı University, Tuzla, Istanbul 34956, Turkey*
[2]*Faculty of Engineering and Natural Sciences, Kadir Has University, Cibali, Istanbul 34083, Turkey*
[3]*Department of Physics, Massachusetts Institute of Technology, Cambridge, Massachusetts 02139, USA*

The left-right chiral and ferromagnetic-antiferromagnetic double spin-glass clock model, with the crucially even number of states $q = 4$ and in three dimensions $d = 3$, has been studied by renormalization-group theory. We find, for the first time to our knowledge, four different spin-glass phases, including conventional, chiral, and quadrupolar spin-glass phases, and phase transitions between spin-glass phases. The chaoses, in the different spin-glass phases and in the phase transitions of the spin-glass phases with the other spin-glass phases, with the non-spin-glass ordered phases, and with the disordered phase, are determined and quantified by Lyapunov exponents. It is seen that the chiral spin-glass phase is the most chaotic spin-glass phase. The calculated phase diagram is also otherwise very rich, including regular and temperature-inverted devil's staircases and reentrances.

I. INTRODUCTION

Spin-glass phases, created by competing frustrated random ferromagnetic and antiferromagnetic interactions, have been known [1] to incorporate a plethora of interesting complex phenomena, not the least being the natural generation chaos [2–4]. Recently, it has been shown [5, 6] that competing left- and right-chiral interactions also create spin-glass phases, even in the absence of competing ferromagnetic and antiferromagnetic interactions. First shown [5] with chiral Potts models [7–11] with the inclusion of quenched randomness, chiral spin glasses were recently extended [6] to clock models with an odd number of states ($q = 5$), resulting in a literally moviesque sequence of phase diagrams, including regular and inverted devil's staircases, a chiral spin-glass phase, and algebraic order.

The chiral clock model work was purposefully initiated [6] with odd number of states q, in order to deal with the complexity of the global phase diagram, since it is known that the odd q models do not show [12] the traditional ferromagnetic-antiferromagnetic spin-glass phase. The current study, on the other hand, is on the random chiral clock model with an even number of states ($q = 4$), which supports the ferromagnetic-antiferromagnetic usual spin-glass phase [12], as well as, as we shall see below, the chiral spin-glass phase and two other new spin-glass phases. A double spin-glass model is constructed, including competing quenched random left-right chiral and ferromagnetic-antiferromagnetic interactions, and solved in three dimensions by renormalization-group theory.

The extremely rich phase diagram includes, to our knowledge for the first time, more than one (four) spin-glass phases on the same phase diagram and three separate spin-glass-to-spin-glass phase transitions. These constitute phase transitions between chaoses. We determine the chaotic behaviors of the spin-glass phases, of the phase transitions between the spin-glass phases, of the phase transitions between the spin-glass phases and the ferromagnetic, antiferromagnetic, quadrupolar, and disordered phases.

II. DOUBLY SPIN GLASS SYSTEM: LEFT-RIGHT CHIRAL AND FERRO-ANTIFERRO INTERACTIONS

The $q-$**state clock spin glass** is composed of unit spins that are confined to a plane and that can only point along q angularly equidistant directions, with Hamiltonian

$$-\beta \mathcal{H} = \sum_{\langle ij \rangle} J_{ij} \vec{s}_i.\vec{s}_j = \sum_{\langle ij \rangle} J_{ij} \cos \theta_{ij}, \qquad (1)$$

where $\beta = 1/k_B T$, $\theta_{ij} = \theta_i - \theta_j$, at each site i the spin angle θ_i takes on the values $(2\pi/q)\sigma_i$ with $\sigma_i = 0, 1, 2, \ldots, (q-1)$, and $\langle ij \rangle$ denotes summation over all nearest-neighbor pairs of sites. As the long-studied ferromagnetic-antiferromagnetic spin-glass system [1], the bond strengths J_{ij}, with quenched (frozen) ferromagnetic-antiferromagnetic randomness, are $+J > 0$ (ferromagnetic) with probability $1-p$ and $-J$ (antiferromagnetic) with probability p, with $0 \leq p \leq 1$. Thus, the ferromagnetic and antiferromagnetic interactions locally compete in frustration centers. Recent studies on ferromagnetic-antiferromagnetic clock spin glasses are in Refs. [12–14].

Doubling the spin-glass effect, in the $q-$**state chiral clock double spin glass** recently introduced (and used in the qualitatively different odd $q = 5$), frustration also occurs via randomly frozen left or right chirality [5]. The Hamiltonian in Eq. (1) is generalized to random local chirality,

$$-\beta \mathcal{H} = \sum_{\langle ij \rangle} [J_{ij} \cos \theta_{ij} + \Delta \, \delta(\theta_{ij} + \eta_{ij} \frac{2\pi}{q})]. \qquad (2)$$

In a cubic lattice, the x, y, or z coordinates increase as sites along the respective coordinate direction are considered. Bond moving as in Fig. 1(a) is done transversely to the bond directions, so that this sequencing is respected. Equivalently, in the corresponding hierarchical lattice, one can always define a direction along the connectivity, for example from left to right in Fig. 1(b), and assign consecutive increasing number labels to the sites. In Eq. (2), for each pair of nearest-neighbor sites $\langle ij \rangle$ the numerical site label j is ahead of i, frozen (quenched) $\eta_{ij} = 1$ (left chirality) or -1 (right chirality), and the delta function $\delta(x) = 1 \, (0)$ for $x = 0 \, (x \neq 0)$. The overall concentrations of left and right chirality are respectively $1 - c$ and c, with $0 \leq c \leq 1$. The strength of the random chiral interaction is Δ/J, with temperature divided out. With no loss of generality, we take $\Delta \geq 0$. Thus, the system is chiral for $\Delta > 0$, chiral-symmetric for $c = 0.5$, chiral-symmetry-broken for $c \neq 0.5$. The global phase diagram is in terms of temperature J^{-1}, antiferromagnetic bond concentration p, random chirality strength Δ/J, and chiral symmetry-breaking concentration c.

III. RENORMALIZATION-GROUP METHOD: MIGDAL-KADANOFF APPROXIMATION AND EXACT HIERARCHICAL LATTICE SOLUTION

Our method has been previously described [6] and used on a qualitatively different model, with qualitatively different results. Thus, we solve the chiral clock double spin-glass model with $q = 4$ states by renormalization-group theory, in $d = 3$ spatial dimensions, with length rescaling factor $b = 3$. We use $b = 3$, as in previous position-space renormalization-group calculations of spin-glass systems, because it treats ferromagnetism and antiferromagnetism on equal footing. Our solution is, simultaneously, the Migdal-Kadanoff approximation [15, 16] for the cubic lattice and the exact solution [17–21] for the $d = 3$ hierarchical lattice based on the repeated self-imbedding of leftmost graph of Fig. 1(b). Fig. 1(a) shows the Migdal-Kadanoff approximate renormalization-group transformation for the cubic lattice, composed of the bond-moving followed by decimation steps. Fig. 1(b) shows the exact renormalization-group transformation for the matching hierarchical lattice. The two procedures yield identical recursion relations. Exact calculations on hierarchical lattices are also currently widely used on a variety of statistical mechanics [22–36] and finance [37] problems.

Under the renormalization-group transformation described below, the Hamiltonian of Eq. (2) maps onto the more general form

$$-\beta\mathcal{H} = \sum_{\langle ij \rangle} V_{ij}(\theta_{ij}), \qquad (3)$$

where $\theta_{ij} = \theta_i - \theta_j$ can take q different values, so that for each pair $< ij >$ of nearest-neighbor sites, there are
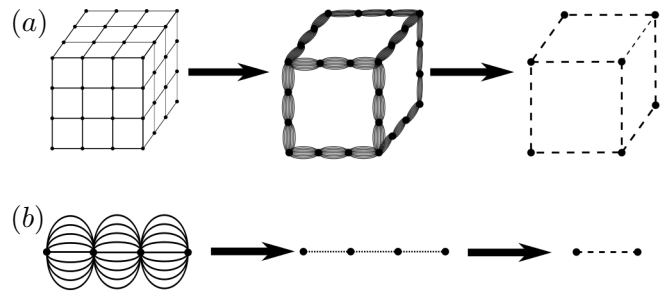

FIG. 1. (a) The Migdal-Kadanoff approximate renormalization-group transformation for the cubic lattice, composed of the bond-moving followed by decimation steps, with the length rescaling factor $b = 3$. The corresponding hierarchical lattice is obtained by the repeated self-imbedding of the leftmost graph in (b). (b) The exact renormalization-group transformation for this $d = 3$ hierarchical lattice. The two procedures yield identical recursion relations.

q = 4 different interaction constants

$$\{V_{ij}(\theta_{ij})\} = \\ \{V_{ij}(0), V_{ij}(\pi/2), V_{ij}(\pi), V_{ij}(3\pi/2)\} \equiv \mathbf{V}_{ij}, \quad (4)$$

which are in general different at each locality (quenched randomness). The largest element of $\{V_{ij}(\theta_{ij})\}$ at each locality $< ij >$ is set to zero, by subtracting the same constant G from all q interaction constants, with no effect on the physics; thus, the $q-1$ other interaction constants are negative.

The local renormalization-group transformation is achieved by the sequence, shown in Fig. 1, of bond movings

$$\widetilde{V}_{ij}(\theta_{ij}) - \widetilde{G} = \sum_{k=1}^{b^{d-1}} V_{ij}^{(k)}(\theta_{ij}), \qquad (5)$$

and decimations

$$e^{V'_{14}(\theta_{14})-G} = \sum_{\theta_2,\theta_3} e^{\widetilde{V}_{12}(\theta_{12})+\widetilde{V}_{23}(\theta_{23})+\widetilde{V}_{34}(\theta_{34})}, \qquad (6)$$

where $\widetilde{G}$ and G are the subtractive constants mentioned above, and prime marks the interaction of the renormalized system.

The starting double-bimodal quenched probability distribution of the interactions, characterized by p and c as described above, is not conserved under rescaling. The renormalized quenched probability distribution of the interactions is obtained by the convolution [38]

$$P'(\mathbf{V}'_{i'j'}) = \int \left\{ \prod_{ij}^{i'j'} d\mathbf{V}_{ij} P(\mathbf{V}_{ij}) \right\} \delta(\mathbf{V}'_{i'j'} - \mathbf{R}(\{\mathbf{V}_{ij}\})), \qquad (7)$$

where $\mathbf{V}_{ij} \equiv \{V_{ij}(\theta_{ij})\}$ as in Eq. (4), $\mathbf{R}(\{\mathbf{V}_{ij}\})$ represents the bond moving and bond decimation given in Eqs.
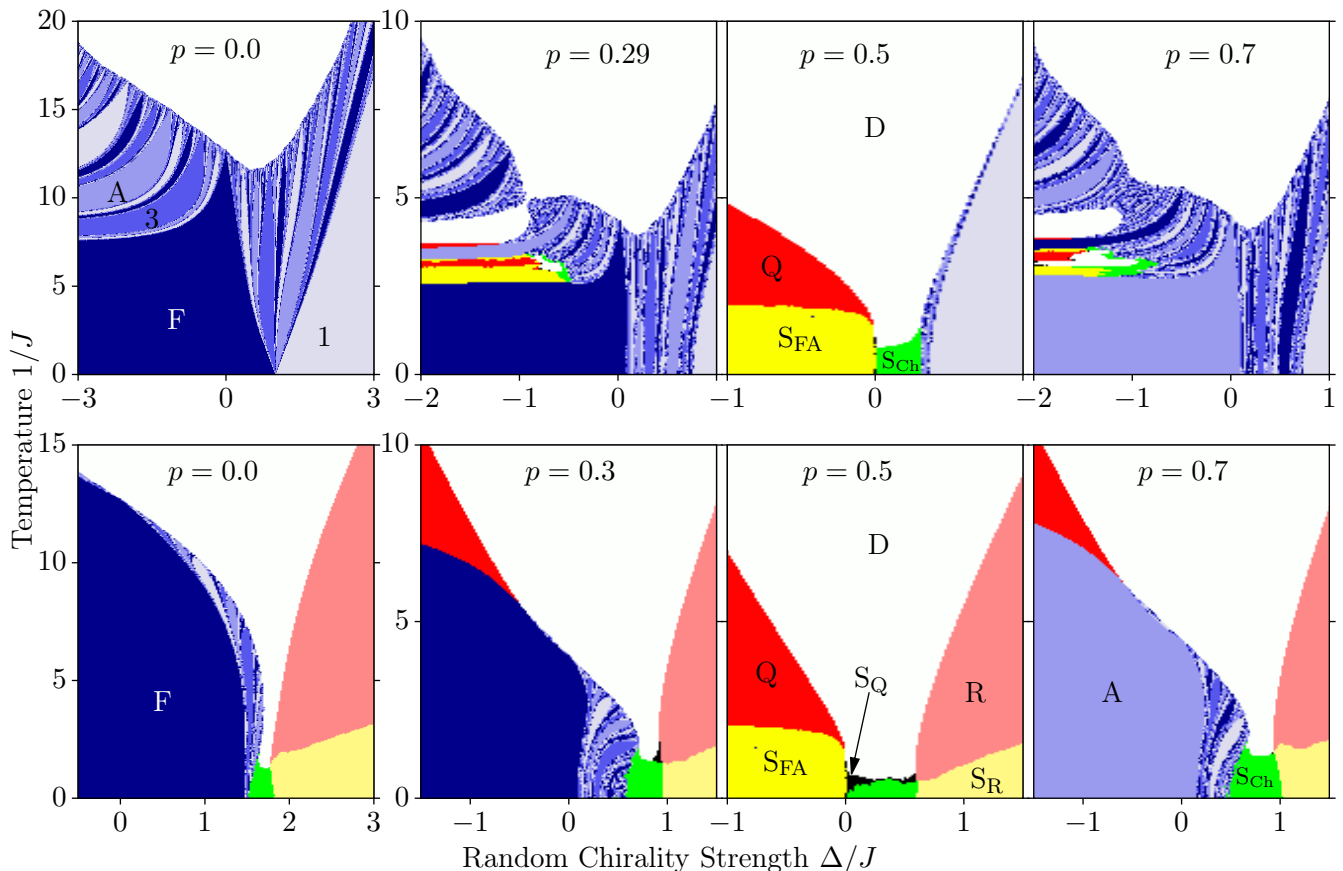
FIG. 2. (Color online) A calculated sequence of phase diagrams for the left chiral ($c = 0$), on the upper side, and quenched random left and right chiral ($c = 0.5$), on the lower side, systems with, in both cases, quenched random ferromagnetic and antiferromagnetic interactions. The horizontal axis is the random chirality strength Δ/J. The consecutive phase diagrams are for different concentrations p of antiferromagnetic interactions. The system exhibits a ferromagnetic phase F, an antiferromagnetic phase A, a multitude of different chiral phases, a quadrupolar phases Q, a "one-step" phase R, and four differently ordered spin-glass phases: the chiral spin-glass S_{CH}, the usual ferromagnetic-antiferromagnetic spin glass S_{FA}, the quadrupolar spin glass S_Q, and S_R. The phase diagrams obtained from p and $1 - p$ are symmetric, since the system has an even number of spin directions. On some of the chiral phases, the $\pi/2$ multiplicity of the asymptotically dominant interaction is indicated. The ferromagnetic and chiral phases accumulate as different devil's staircases at their boundary with the disordered (D) phase.

(5) and (6), and primes refer to the renormalized system. Similar previous studies, on other spin-glass systems, are in Refs. [12, 13, 39–46]. For numerical practicality the bond moving and decimation of Eqs. (5) and (6) are achieved by a sequential pairwise combination of interactions, each pairwise combination leading to an intermediate probability distribution resulting from a pairwise convolution as in Eq. (7).

We effect this procedure numerically, first starting with the initial double delta distribution of Eq. (2) giving 4 possible interactions quenched randomly distributed throughout the system, and generating 1000 interactions that embody the quenched probability distribution resulting from the pairwise combination. Each of the generated 1000 interactions is described by $q = 4$ interaction constants, as explained above [Eq. (4)]. At each subsequent pairwise convolution as in Eq. (7), 1000 randomly chosen pairs, representing quenched random neighbors in the lattice, are matched by (5) or (6), and a new set of 1000 interactions is produced.

Our calculation simply consists in following the recursion relations, Eqs.(5-7) to the various fixed points and thereby mapping the initial conditions that are the basins of attraction of the various fixed points. This map is the phase diagram: The different thermodynamic phases of the system are identified by the different asymptotic renormalization-group flows of the quenched probability distribution $P(\mathbf{V}_{ij})$. Two renormalization-group trajectories starting at each side of a phase boundary point diverge from each other, flowing towards the phase sinks (completely stable fixed points) of their respective phases. Thus, the phase boundary point between two phases is readily obtained to the accuracy of the figures. We are therefore able to calculate the global phase diagram of the (importantly even) $q = 4$ chiral clock double spin-glass model.
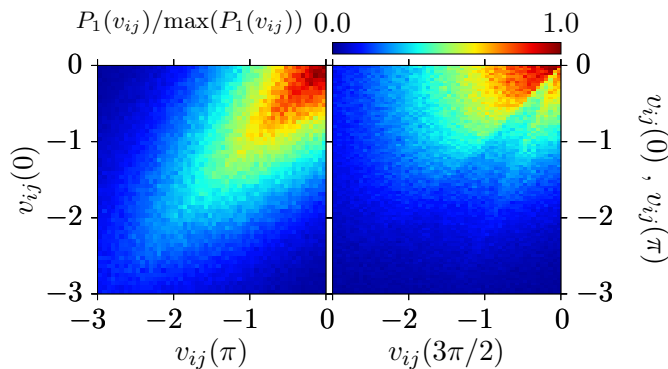
FIG. 3. (Color online) Asymptotic fixed distribution of the chiral spin-glass phase S_{Ch}. The part of the fixed distribution $P_1(\mathbf{V}_{ij})$, for the interactions $\mathbf{V}_{ij}$ in which $V_{ij}(\pi/2)$ is maximum and therefore 0 (and the other three interactions are negative) is shown in this figure, with $v_{ij}(\theta) = V_{ij}(\theta)/\langle|V_{ij}(\theta)|\rangle$. The projections of $P_1(\mathbf{V}_{ij})$ onto two of its three arguments are shown in each panel of this figure. The other three $P_\sigma(\mathbf{V}_{ij})$ have the same fixed distribution. Thus chirality is broken locally but not globally, just as, in the long-time studied ferromagnetic-antiferromagnetic spin glasses, spin-direction symmetry breaking is local but not global (i.e., the local magnetization is non-zero, the global magnetization is zero).
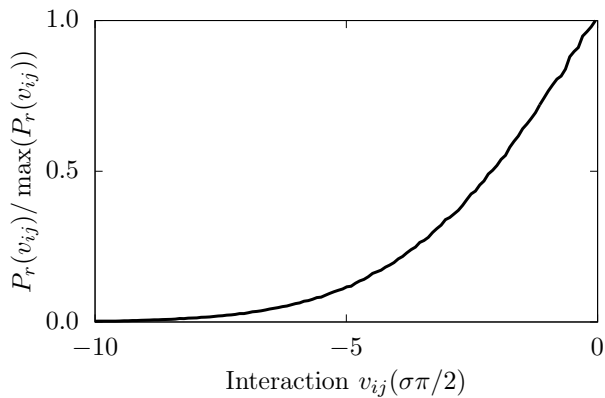

FIG. 4. Asymptotic fixed distributions of 3 different spin-glass phases, with $v_{ij}(\theta) = V_{ij}(\theta)/\langle|V_{ij}(\theta)|\rangle$. For the ferromagnetic-antiferromagnetic spin-glass S_{FA} phase, $r = 0, \sigma = 2$ and $r = 2, \sigma = 0$. The other two angles do not occur. For the quadrupolar spin-glass S_Q phase, $r = 0, \sigma = 1$ and $r = 1, \sigma = 0$, with $V_{ij}(0) = V_{ij}(\pi)$ and $V_{ij}(\pi/2) = V_{ij}(3\pi/2)$. For the spin-glass S_R phase, $r = 1, \sigma = 3$ and $r = 3, \sigma = 1$. The other two angles do not occur. The $v_{ij}(0) = v_{ij}(\pi)$ curve obtained from the left panel of Fig. 3 also matches the curve here.

IV.   GLOBAL PHASE DIAGRAM: MULTIPLE SPIN-GLASS PHASES

The global phase diagram of the $q = 4$ state chiral clock double spin-glass model in $d = 3$ spatial dimensions, in temperature J^{-1}, antiferromagnetic bond concentration p, random chirality strength Δ/J, and right-chirality concentration c, is a four-dimensional object, so that only the cross-sections of the global phase diagram are exhibited.

Figs. 2 show a calculated sequence of phase diagram cross sections for the left-chiral ($c = 0$), on the upper side, and quenched random left- and right-chiral ($c = 0.5$), on the lower side, systems with in both cases quenched random ferromagnetic and antiferromagnetic interactions. The horizontal axis is the random chirality strength Δ/J (See Eq.(2)). The consecutive phase diagrams are for different concentrations p of antiferromagnetic interactions. The system exhibits a disordered phase (D), a ferromagnetic phase (F), a conventionally ordered (in contrast to the algebraically ordered for $q = 5$) antiferromagnetic phase (A), a quadrupolar phase (Q), a new "one-step" phase (R), a multitude of different chiral phases, and four different spin-glass phases (S_{Ch}, S_{FA}, S_Q, S_R) including spin-glass-to-spin-glass phase transitions. The ferromagnetic and different chiral phases accumulate as conventional and temperature-inverted (abutting to the reentrant [47–51] disordered phase) devil's staircases [52, 53] at their boundary with the disordered (D) phase. This accumulation occurs at all scales of phase diagram space (i.e., at all magnifications of the phase diagram figure).

Unlike the odd q case of $q = 5$, which incorporates built-in entropy [6] even without any quenched randomness, no algebraically ordered phase [54, 55] occurs in this even q case of $q = 4$. The devil's staircases of the chiral phases is again seen. Most interestingly, quadrupolar and "one-step" phases, different spin-glass phases for the first time in the same phase diagram, and spin-glass-to-spin-glass direct phase transitions are seen. The phases and phase boundaries involving spin glassiness are tracked through the calculated Lyapunov exponents of their chaos.

In all ordered phases, the renormalization-group trajectories flow to strong (infinite) coupling. In the ferromagnetic phase, under renormalization-group transformations, the interaction $V_{ij}(0)$ becomes asymptotically dominant. In the antiferromagnetic phase, under renormalization-group transformations, the interaction $V_{ij}(\pi)$ becomes asymptotically dominant. In the quadrupolar phase Q, the interactions $V_{ij}(0)$ and $V_{ij}(\pi)$ become asymptotically dominant and equal. Thus, there are two such quadrupolar phases, namely along the spin directions $\pm x$ and $\pm y$, with the additional (factorized) trivial degeneracy of $\pm$ spin direction at each site. In the new "one-step phase" R, the interactions $V_{ij}(+\pi/2)$ and $V_{ij}(-\pi/2)$ become asymptotically dominant and equal. Thus, in such a phase, the average local spins can span all spin directions, taking $\pm\pi/2$ steps from one spin to the next in the renormalized systems.

In the chiral phases, in the renormalization-group trajectories, one of the chiral interactions from the right-hand side of Eq. (4), $\{V_{ij}(\pi/2), V_{ij}(3\pi/2)\}$, becomes asymptotically dominant. However, in each of the separate chiral phases, it takes a characteristic number n of renormalization-group transformations, namely a length scale of 3^n, to reach the dominance of one chi-
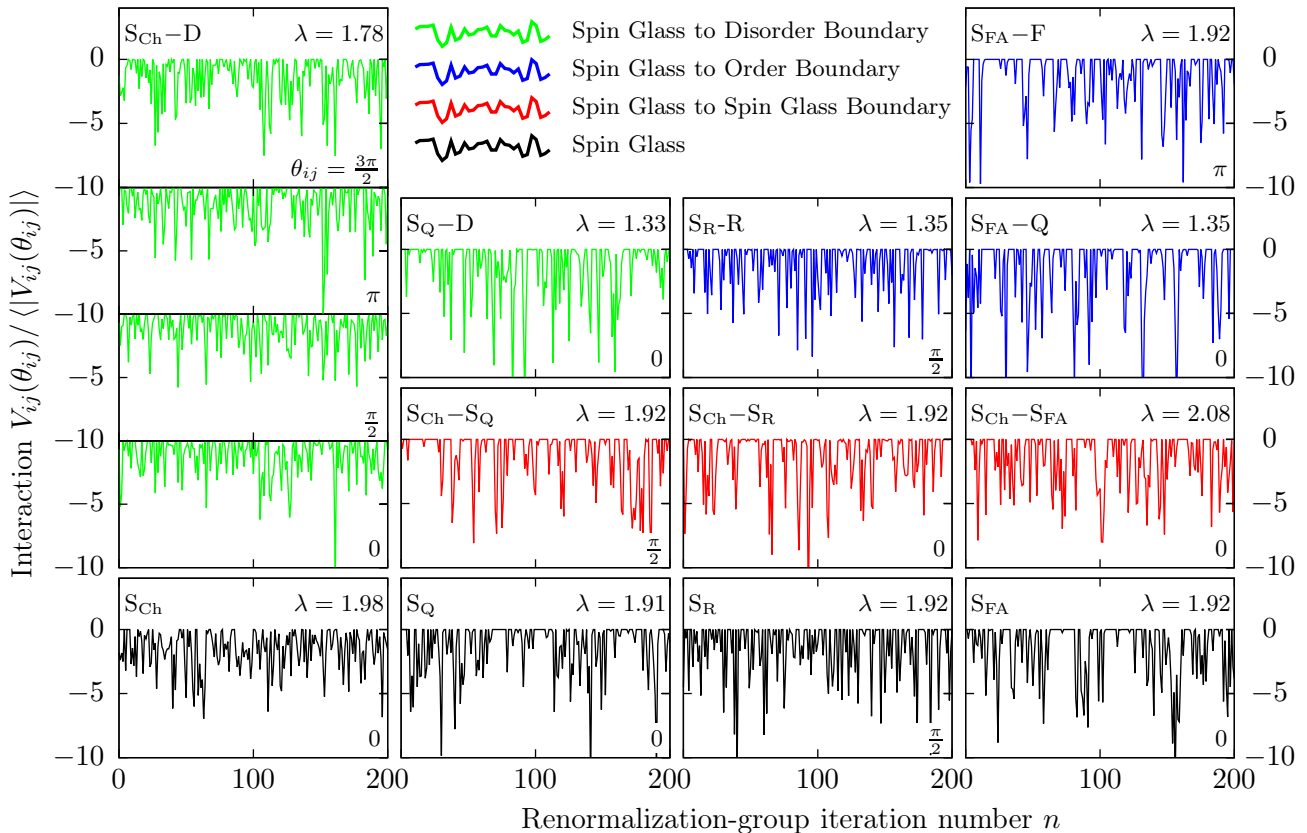
FIG. 5. Chaotic renormalization-group trajectories of the four different spin-glass phases (black), of the phase boundaries of the spin-glass phases with other spin-glass phases (red), with non-spin-glass ordered (blue) and disordered (green) phases. The phase boundary chaoses of each spin-glass phase are given in their corresponding vertically aligned panels. In each case, only one of the four interactions $V_{ij}(0), V_{ij}(\pi/2), V_{ij}(\pi), V_{ij}(3\pi/2)$ at a given location $\langle ij \rangle$, under consecutive renormalization-group transformations, is shown, except, for illustration, all four interactions are shown for the chaos at the phase transition between the chiral spin-glass and disordered phases. The θ_{ij} angular value of each interaction $V_{ij}(\theta_{ij})$ is indicated in the figure panels, as well as the Lyapunov exponent λ calculated from the chaotic sequence under renormalization-group transformations. The Lyapunov exponent is calculated over 1,000 renormalization-group iterations, after throwing out the first 200 iterations. Inside all four spin-glass phases, the average interaction diverges as $<|V|>\sim b^{y_R n}$, where n is the number of renormalization-group iterations and $y_R = 0.25$ is the runaway exponent. At the $S_{Ch}-S_R$, $S_{Ch}-S_Q$, $S_{FA}-A$, $S_{FA}-F$ phase boundaries, $y_R = 0.25$ also. At the $S_{Ch}-S_{FA}$ phase boundary, $y_R = 0.11$ for $V_{ij}(0), V_{ij}(\pi)$ and $y_R = 0.25$ for $V_{ij}(\pi/2), V_{ij}(3\pi/2)$. At the phase boundaries of the spin-glass phases with some non-spin-glass-ordered and disordered phases, the average interaction remains non-divergent, fixed at $<V>= -0.34$ for $S_{FA}-Q$, S_R-R, S_Q-D and $<V>= -1.07$ for $S_{Ch}-D$. As indicated by the Lyapunov exponents, chaos is stronger inside the chiral spin-glass phase.

ral interaction. This distinct number of iterations, namely scale changes, determines, by tracing back to the periodic sequence in the original lattice, the pitch of the chiral phase in the original unrenormalized system. Thus, the chiral phases in the original unrenormalized system, with distinct chiral pitches, are distinct phases. After the dominance of one chiral interaction, the renormalization-group trajectory follows the periodic sequence $V_{ij}(\pi/2) \to V_{ij}(3\pi/2) \to V_{ij}(\pi/2)$ resulting from matching $q = 4$ and $b = 3$.

The renormalization-group trajectories starting in the spin-glass phases, unlike those in the ferromagnetic, antiferromagneric, quadrupolar, "one-step", and chiral phases, do not have the asymptotic behavior where at

any scale one potential $V(\theta)$ is dominant. These trajectories of the spin-glass phases asymptotically go to a strong-coupling fixed probability distribution $P(\mathbf{V}_{ij})$ which assigns non-zero probabilities to a distribution of $\mathbf{V}_{ij}$ values, with no single $V_{ij}(\theta)$ being dominant. These distributions are shown in Figs. 3 and 4. Different asymptotic fixed probability distributions indicate different spin-glass phases.

Since, at each locality, the largest interaction in $\{V_{ij}(0), V_{ij}(\pi/2), V_{ij}(\pi), V_{ij}(3\pi/2)\}$ is set to zero and the three other interactions are thus made negative, by subtracting the same constant from all four interactions without affecting the physics, the quenched probability distribution $P(\mathbf{V}_{ij})$, a function of four variables, is ac-

tually composed of four functions $P_\sigma(\mathbf{V}_{ij})$ of three variables, each such function corresponding to one of the interactions being zero and the other three, arguments of the function, being negative. Figs. 3 and 4 show the latter functions.

In Fig. 3 for the spin-glass phase S_{Ch}, the part of the fixed distribution, $P_1(\mathbf{V}_{ij})$, for the interactions $\mathbf{V}_{ij}$ in which $V_{ij}(\pi/2)$ is maximum and therefore 0 (and the other three interactions are negative) is shown. The projections of $P_1(\mathbf{V}_{ij})$ onto two of its three arguments are shown in each panel of Fig. 3. The other three $P_\sigma(\mathbf{V}_{ij})$ have the same fixed distribution. Thus, chirality is broken locally, but not globally, just as, in the long-time studied ferromagnetic-antiferromagnetic spin glasses, spin-direction symmetry breaking is local but not global (i.e., the local magnetization is non-zero, the global magnetization is zero). The asymptotic fixed distribution of the phase S_{Ch}, given in Fig. 3, assigns non-zero probabilities to a continuum of values for all four interactions $\{V_{ij}(0), V_{ij}(\pi/2), V_{ij}(\pi), V_{ij}(3\pi/2)\}$. The phase S_{Ch} is therefore a chiral spin-glass phase. The similar chiral spin-glass phase has been seen previously, as the sole spin-glass phase, for the odd $q = 5$.[6]. The chiral spin-glass phase occurs even when there is no competing ferromagnetic-antiferromagnetic interactions.[5, 6]

As seen in Fig. 4, in the asymptotic fixed distribution of the spin-glass phase S_{FA}, non-zero probabilities are assigned to a continuum of values of $\{V_{ij}(0), V_{ij}(\pi)\}$. Fig. 4 shows the fixed distribution values $P_0(V_{ij}(\pi))$ for $V_{ij}(0)$ maximum and therefore set to zero. Completing the asymptotic fixed distribution of S_{FA} is an identical function $P_2(V_{ij}(0))$ for $V_{ij}(\pi)$ maximum and therefore set to zero. At this fixed distribution, the values of $V_{ij}(\pi/2)$ and $V_{ij}(3\pi/2)$ diverge to negative infinity, so that these angles do not occur. Thus, S_{FA} is the long-studied [1] spin-glass phase of competing ferromagnetic and antiferromagnetic interactions.

Fig. 4 also shows the asymptotic fixed distribution of the spin-glass phase S_R, with the functions $P_1(V_{ij}(3\pi/2))$ for $V_{ij}(\pi/2)$ maximum (and therefore set to zero) and $P_3(V_{ij}(\pi/2))$ for $V_{ij}(3\pi/2)$ maximum (and therefore set to zero). Again, the other two angles do not occur at this asymptotic fixed distribution. Furthermore, Fig. 4 also shows the asymptotic fixed distribution of the spin-glass phase S_Q, with the functions $P_0(V_{ij}(\pi/2))$ and $P_1(V_{ij}(0))$, with $V_{ij}(0) = V_{ij}(\pi)$ and $V_{ij}(\pi/2) = V_{ij}(3\pi/2)$. Thus, this fixed distribution does not locally distinguish between $\pm$ spin directions and is thus a quadrupolar spin-glass phase.

In fact, the $v_{ij}(0) = v_{ij}(p)$ curve obtained from the left panel of Fig. 3 also matches the curve here. The three fixed distributions given in Fig. 4 exhibit the same numerical curve, but refer to widely different interactions. Thus, they underpin different spin-glass phases.

V. PHASE TRANSITIONS BETWEEN CHAOS

Another distinctive mechanism, that of chaos under scale change [2–4] or, equivalently [13], chaos under spatial translation, occurs within the spin-glass phase and differently at the spin-glass phase boundary [13], in systems with competing ferromagnetic and antiferromagnetic interactions [2–4, 13, 45, 56–82] and, more recently, with competing left- and right-chiral interactions [5, 6]. The physical hierarchical lattice that we solve here is an infinite system, where 1000 quadruplets $\{V_{ij}(0), V_{ij}(\pi/2), V_{ij}(\pi), V_{ij}(3\pi/2)\}$ are randomly distributed over the lattice bond positions. Thus, we can fix our attention to one lattice position and monitor how the quadruplet at that position evolves under renormalization-group transformation, as it merges with its neighbors through bond moving [Eq. (5)] and decimation [Eq. (6)], and thereby calculate the Lyapunov exponent [13, 45], which when positive is the measure of the strength of chaos.

Fig. 5 gives the asymptotic chaotic renormalization-group trajectories of the four different spin-glass phases and of the phase boundaries between the spin-glass phases with other spin-glass phases, with the non-spin-glass ordered phases and the disordered phase. The chaotic trajectories found here are similar to those found in traditional (Ising) spin-glasses [13, 45], with of course different Lyapunov exponents seen below. The four interactions $V_{ij}(0), V_{ij}(\pi/), V_{ij}(\pi), V_{ij}(3\pi/2)$ at a given location $< ij >$, under consecutive renormalization-group transformations, are shown in Fig. 5. As noted, chaos is measured by the Lyapunov exponent [13, 45, 73, 83, 84], which we have previously [6] generalized, by the matrix form, to multi-interaction cases:

$$\lambda = \lim_{n \to \infty} \frac{1}{n} \ln \left| \mathcal{E} \left(\prod_{k=0}^{n-1} \frac{d\mathbf{v}_{k+1}}{d\mathbf{v}_k} \right) \right|, \qquad (8)$$

where the function $\mathcal{E}(\mathbf{M})$ gives the largest eigenvalue of its matrix argument $\mathbf{M}$ and the vector $\mathbf{v}_k$ is

$$\mathbf{v}_k = \{v_{ij}(0), v_{ij}(\pi/2), v_{ij}(\pi), v_{ij}(3\pi/2)\}, \qquad (9)$$

with $v_{ij}(\theta) = V_{ij}(\theta)/ < |V_{ij}(\theta)| >$, at step k of the renormalization-group trajectory. The product in Eq. (8) is to be taken within the asymptotic chaotic band, which is renormalization-group stable or unstable for the spin-glass phase or its boundaries, respectively. Thus, we throw out the first 200 renormalization-group iterations to eliminate the transient points outside of, but leading to the chaotic band. Subsequently, typically using 1,000 renormalization-group iterations in the product in Eq. (8) assures the convergence of the Lyapunov exponent value λ.

Spin-glass chaos occurs for $\lambda > 0$ [73] and the more positive λ, the stronger is chaos, as seen for example in the progressions in Figs. 6 and 7 of Ref. [45]. Inside all four spin-glass phases, the average interaction

diverges as $< |V| > \sim b^{y_R n}$, where n is the number of renormalization-group iterations and $y_R = 0.25$ is the runaway exponent. In the non-spin-glass ordered phases, the runaway exponent value is $y_R = d - 1 = 3$ [85].

At the S_{Ch}−S_R, S_{Ch}−S_Q, $S_{FA} - F$ and its symmetric S_{FA}−A phase boundaries, $y_R = 0.25$ also. At the S_{Ch}−S_{FA} phase boundary, $y_R = 0.11$ for $V_{ij}(0), V_{ij}(\pi)$ and $y_R = 0.25$ for $V_{ij}(\pi/2), V_{ij}(3\pi/2)$. At the phase boundaries of the spin-glass phases with some non-spin-glass ordered and disordered phases, the average interaction remains non-divergent, fixed at $< V > = -0.34$ for S_{FA}−Q, S_R−R, S_Q−D and $< V > = -1.07$ for S_{Ch}−D. As indicated by the Lyapunov exponents, chaos is stronger inside the spin-glass phase than at its phase boundaries with non-spin-glass phases.

As expected from the asymptotic fixed distribution analysis given above, the three spin-glass phases S_{FA}, S_Q, S_R and the phase transitions between these phases have the same Lyapunov exponent $\lambda = 1.92$ and therefore the same degree of chaos. The chiral spin-glass S_{Ch} has more chaos ($\lambda = 1.98$) from the other three spin-glass phases. The phase transition between the chiral spin-glass phase S_{Ch} and the other three spin-glass phases is a phase transition between different types of chaos. This phase transition itself of course exhibits chaos, as do all spin-glass phase boundaries.

VI. CONCLUSION

The left-right chiral and ferromagnetic-antiferromagnetic double spin-glass clock model, with the crucially even number of states $q = 4$ and in three dimensions $d = 3$, has been solved by renormalization-group theory that is approximate for the cubic lattice and exact for the corresponding hierarchical lattice. We find in the same phase diagram, for the first time to our knowledge, four different spin-glass phases, including conventional, chiral, and quadrupolar spin-glass phases, and phase transitions between spin-glass phases. The chaoses, in the different spin-glass phases and in the phase transitions of the spin-glass phases with the other spin-glass phases, the non-spin-glass ordered phases, and the disordered phase, are determined and quantified by Lyapunov exponents. It is seen that the chiral spin-glass phase is the most chaotic spin-glass phase. The calculated phase diagram is also otherwise very rich, including regular and temperatue-inverted devil's staircases and reentrances.

[1] H. Nishimori, *Statistical Physics of Spin Glasses and Information Processing* (Oxford University Press, Oxford, 2001).

[2] S. R. McKay, A. N. Berker, and S. Kirkpatrick, Phys. Rev. Lett. **48**, 767 (1982).

[3] S. R. McKay, A. N. Berker, and S. Kirkpatrick, J. Appl. Phys. **53**, 7974 (1982).

[4] A. N. Berker and S. R. McKay, J. Stat. Phys. **36**, 787 (1984).

[5] T. Çağlar and A. N. Berker, Phys. Rev. E **94**, 032121 (2016).

[6] T. Çağlar and A. N. Berker, Phys. Rev. E **95**, 042125 (2017).

[7] S. Ostlund, Phys. Rev. **24**, 398 (1981).

[8] M. Kardar and A. N. Berker, Phys. Rev. Lett. **48**, 1552 (1982).

[9] D. A. Huse and M. E. Fisher, Phys. Rev. Lett. **49**, 793 (1982).

[10] D. A. Huse and M. E. Fisher, Phys. Rev. **29**, 239 (1984).

[11] R. G. Caflisch, A. N. Berker, and M. Kardar, Phys. Rev. B **31**, 4527 (1985).

[12] E. Ilker and A. N. Berker, Phys. Rev. E **90**, 062112 (2014).

[13] E. Ilker and A. N. Berker, Phys. Rev. E **87**, 032124 (2013).

[14] C. Lupo and F. Ricci-Tersenghi, Phys. Rev. B **95**, 054433 (2017).

[15] A. A. Migdal, Zh. Eksp. Teor. Fiz. **69**, 1457 (1975) [Sov. Phys. JETP **42**, 743 (1976)].

[16] L. P. Kadanoff, Ann. Phys. (N.Y.) **100**, 359 (1976).

[17] A. N. Berker and S. Ostlund, J. Phys. C **12**, 4961 (1979).

[18] R. B. Griffiths and M. Kaufman, Phys. Rev. B **26**, 5022R (1982).

[19] M. Kaufman and R. B. Griffiths, Phys. Rev. B **30**, 244 (1984).

[20] S. R. McKay and A. N. Berker, Phys. Rev. B **29**, 1315 (1984).

[21] M. Hinczewski and A. N. Berker, Phys. Rev. E **73**, 066126 (2006).

[22] B. Derrida and G. Giacomin, J. Stat. Phys. **154**, 286 (2014).

[23] M. F. Thorpe and R. B. Stinchcombe, Philos. Trans. Royal Soc. A - Math. Phys. Eng. Sciences **372**, 20120038 (2014).

[24] A. Efrat and M. Schwartz, Physica **414**, 137 (2014).

[25] C. Monthus and T. Garel, Phys. Rev. B **89**, 184408 (2014).

[26] M. L. Lyra, F. A. B. F. de Moura, I. N. de Oliveira, and M. Serva, Phys. Rev. E **89**, 052133 (2014).

[27] Y.-L. Xu, X. Zhang, Z.-Q. Liu, K. Xiang-Mu, and R. Ting-Qi, Eur. Phys. J. B **87**, 132 (2014).

[28] V. S. T. Silva, R. F. S. Andrade, and S. R. Salinas, Phys. Rev. E **90**, 052112 (2014).

[29] S. Boettcher, S. Falkner, and R. Portugal, Phys. Rev. A **91** 052330 (2015).

[30] S. Boettcher and C. T. Brunson, Eur. Phys. Lett. **110**, 26005 (2015).

[31] Y. Hirose, A. Ogushi, and Y. Fukumoto, J. Phys. Soc. Japan **84**, 104705 (2015).

[32] S. Boettcher and L. Shanshan, J. Phys. A **48**, 415001 (2015).

[33] A. Nandy and A. Chakrabarti, Phys. Lett. **379**, 43 (2015).

[34] S. Li and S. Boettcher, Phys. Rev. A **95**, 032301 (2017).

[35] P. Bleher, M. Lyubich, and R. Roeder, J. Mathematiques Pures et Appliquées **107**, 491 (2017).

[36] H. Li and Z. Zhang, Theoretical Comp. Sci. **675**, 64 (2017).

[37] S. J. Sirca and M. Omladic, ARS Mathematica Contemporanea **13**, 63 (2017).

[38] D. Andelman and A. N. Berker, Phys. Rev. B **29**, 2630 (1984).

[39] M. J. P. Gingras and E. S. Sørensen, Phys. Rev. B. **46**, 3441 (1992).

[40] G. Migliorini and A. N. Berker, Phys. Rev. B. **57**, 426 (1998).

[41] M. J. P. Gingras and E. S. Sørensen, Phys. Rev. B. **57**, 10264 (1998).

[42] C. N. Kaplan and A. N. Berker, Phys. Rev. Lett. **100**, 027204 (2008).

[43] C. Güven, A. N. Berker, M. Hinczewski, and H. Nishimori, Phys. Rev. E **77**, 061110 (2008).

[44] M. Ohzeki, H. Nishimori, and A. N. Berker, Phys. Rev. E **77**, 061116 (2008).

[45] E. Ilker and A. N. Berker, Phys. Rev. E **89**, 042139 (2014).

[46] M. Demirtaş, A. Tuncer, and A. N. Berker, Phys. Rev. E **92**, 022136 (2015).

[47] P. E. Cladis, Phys. Rev. Lett. **35**, 48 (1975).

[48] F. Hardouin, A. M. Levelut, M. F. Achard, and G. Sigaud, J. Chim. Phys. **80**, 53 (1983).

[49] J. O. Indekeu, A. N. Berker, C. Chiang, and C. W. Garland, Phys. Rev. A **35**, 1371 (1987).

[50] R. R. Netz and A. N. Berker, Phys. Rev. Lett. **68**, 333 (1992).

[51] S. Kumari and S. Singh, Phase Transitions **88**, 1225 (2015).

[52] P. Bak and R. Bruinsma, Phys. Rev. Lett. **49**, 249 (1982).

[53] A. Fukuda, Y. Takanishi, T. Isozaki, K. Ishikawa, and H. Takezoe, J. Mat. Chem. **4**, 997 (1994).

[54] A. N. Berker and L. P. Kadanoff, J. Phys. A **13**, L259 (1980).

[55] A. N. Berker and L. P. Kadanoff, J. Phys. A **13**, 3786 (1980).

[56] A. J. Bray and M. A. Moore, Phys. Rev. Lett. **58**, 57 (1987).

[57] E. J. Hartford and S. R. McKay, J. Appl. Phys. 70, 6068 (1991).

[58] M. Nifle and H. J. Hilhorst, Phys. Rev. Lett. **68**, 2992 (1992).

[59] M. Nifle and H. J. Hilhorst, Physica A **194**, 462 (1993).

[60] M. Cieplak, M. S. Li, and J. R. Banavar, Phys. Rev. B **47**, 5022 (1993).

[61] F. Krzakala, Europhys. Lett. **66**, 847 (2004).

[62] F. Krzakala and J. P. Bouchaud, Europhys. Lett. **72**, 472 (2005).

[63] M. Sasaki, K. Hukushima, H. Yoshino, and H. Takayama, Phys. Rev. Lett. **95**, 267203 (2005).

[64] J. Lukic, E. Marinari, O. C. Martin, and S. Sabatini, J. Stat. Mech.: Theory Exp. L10001 (2006).

[65] P. Le Doussal, Phys. Rev. Lett. **96**, 235702 (2006).

[66] T. Rizzo and H. Yoshino, Phys. Rev. B **73**, 064416 (2006).

[67] H. G. Katzgraber and F. Krzakala, Phys. Rev. Lett. **98**, 017201 (2007).

[68] H. Yoshino and T. Rizzo, Phys. Rev. B **77**, 104429 (2008).

[69] J. H. Pixley and A. P. Young, Phys Rev B **78**, 014419 (2008).

[70] T. Aspelmeier, Phys. Rev. Lett. **100**, 117205 (2008).

[71] T. Aspelmeier, J. Phys. A **41**, 205005 (2008).

[72] T. Mora and L. Zdeborova, J. Stat. Phys. **131**, 1121 (2008).

[73] N. Aral and A. N. Berker, Phys. Rev. B **79**, 014434 (2009).

[74] Q. H. Chen, Phys. Rev. B **80**, 144420 (2009).

[75] T. Jörg and F. Krzakala, J. Stat. Mech.: Theory Exp. L01001 (2012).

[76] W. de Lima, G. Camelo-Neto, and S. Coutinho, Phys. Lett. A **377**, 2851 (2013).

[77] W. Wang, J. Machta, and H. G. Katzgraber, Phys. Rev. B **92**, 094410 (2015).

[78] V. Martin-Mayor and I. Hen, Scientific Repts. **5**, 15324 (2015).

[79] Z. Zhu, A. J. Ochoa, S. Schnabel, F. Hamze, and H. G. Katzgraber, Phys. Rev. A **93**, 012317 (2016).

[80] W. Wang, J. Machta, and H. G. Katzgraber, Phys. Rev. B **93**, 224414 (2016).

[81] J. Marshall, V. Martin-Mayor, and I. Hen, Phys. Rev. A **94**, 012320 (2016).

[82] L. A. Fernandez, E. Marinari, V. Martin-Mayor, G. Parisi, and D. Yllanes, J. Stat. Mech.: Theory Exp., 123301 (2016).

[83] P. Collet and J.-P. Eckmann, *Iterated Maps on the Interval as Dynamical Systems* (Birkhäuser, Boston, 1980).

[84] R. C. Hilborn, *Chaos and Nonlinear Dynamics*, 2nd ed. (Oxford University Press, New York, 2003).

[85] A. N. Berker, Phys. Rev. B **29**, 5243 (1984).